Article

Reduction of Cancer Stem Cells and Invasiveness of Human Melanoma and Breast Cancer by Cucurbitacin B from *Lagenaria siceraria*

Cheng-Chen Huang [1],*, Kiera K. Balding [1], Sydney J. Zimmerman [1], Che-Yuan Chang [2], Si-Min Lu [2] and Hui-Chi Huang [2,3],*

[1] Biology Department, University of Wisconsin-River Falls, River Falls, WI 54022, USA
[2] Department of Chinese Pharmaceutical Sciences and Chinese Medicine Resources, China Medical University, Taichung 40402, Taiwan
[3] Master Program for Food and Drug Safety, China Medical University, Taichung 40402, Taiwan
*   Correspondence: cheng-chen.huang@uwrf.edu (C.-C.H.); hchuang@mail.cmu.edu.tw (H.-C.H.); Tel.: +715-425-4276 (C.-C.H.); +886-4-2205-3366 (ext. 5211) (H.-C.H.); Fax: +715-425-0378 (C.-C.H.)

Abstract: Cucurbitacins are secondary metabolites that are commonly found in the Cucurbitacae family. Many biological properties have been reported for cucurbitacins, including anti-inflammatory, antioxidant, antiviral, anti-malaria, and anticancer properties. While studies for the anticancer property of cucurbitacins focus mostly on the cell-cycle progression and apoptosis, no study has considered the effect of cucurbitacin on other cancer behaviors. Here, we report cell-proliferation-based drug testing on random herbal extracts leading to the identification of cucurbitacin B as an anticancer compound. Interestingly, cucurbitacin B had no effect on the proliferation of rat embryonic myoblast cells. We also found that cucurbitacin B significantly reduced the invasiveness of at least two highly metastatic breast cancer and melanoma cells. Using known cancer stem-cell markers, we observed a significant reduction of the melanoma stem cells. Molecularly, cucurbitacin B caused reduction of the metastasis-promoting gene Snail in melanoma and one of the cancer stem cell markers, ALDH1A1 (aldehyde dehydrogenase 1 A1), in breast cancer. Finally, we report the potential toxicity of cucurbitacin B in developing skin tissue and the olfactory organ using zebrafish embryo. In summary, our study suggests the potential use of cucurbitacin B for cancer metastasis and relapse treatment.

Keywords: cancer invasiveness; cancer stem cells; melanoma; breast cancer; cucurbitacin

1. Introduction

With cancers being the second leading cause of death worldwide and metastasis accounting for 90% of all cancer death [1], it seems obvious that developing cancer therapy targeting metastasis would be one of the most effective life-saving approaches. It has been well established that cancer stem cells (CSCs) are the source of metastasis. CSCs are cancer cells that possess stem cell properties and, thus, they are able to renew, proliferate, and differentiate cancer tissue [2]. They have been found in almost all cancers, ranging from 0.02% to 25% depending on the cancer type [3]. CSCs have also been found, in many studies, to be invasive and resistant to conventional chemotherapies, making CSCs the biggest challenge in cancer therapy. Fortunately, CSCs can be detected and isolated by so-called CSC markers, allowing the number of CSCs to be monitored and for cancer prognosis upon treatment to be predicted [4]. Thus, cancer treatment with therapeutics that reduce the stem cell population will decrease the probability of metastasis and other problems related to CSCs, such as tumor relapse and chemotherapeutic resistance [5].

Metastasis typically involves the cellular change called epithelial–mesenchymal transition (EMT), which allows epithelial cancers to become individual migratory and invasive

mesenchymal cells. Several proteins that are specifically associated with epithelia, such as E-cadherin, have been found to be anti-metastasic. Likewise, some proteins that are associated with mesenchymal cells, such as vimentin, have been found to be pro-metastasic [6]. In addition, some transcription factors were reported to be pro-metastasic, such as Twist and Snail [7]. These transcription factors are often associated with CSCs' stemness as well. This EMT–metastasis transcription factors-CSCs network will apparently be the primary target in metastasis study and treatment.

Plant secondary metabolites are an important source for cancer and other therapies. In fact, several widely prescribed cancer medications are derived from plants, such as the well-known paclitaxel (or Taxol), which is derived from the bark of the Pacific yew tree (*Taxus brevifolia*), and vinblastine from the flowering herb periwinkle (*Catharanthus roseus*). Both paclitaxel and vinblastine were found to target the microtubule system and inhibit mitosis. As they interfere with the general cell-division device, these natural compounds strongly inhibit the proliferation of cancer cells and, unfortunately, non-cancer cells, causing severe side effects that are commonly seen in many cytotoxic chemotherapeutic drugs. CSCs are able to escape from these types of cytotoxic drugs because they are often in a quiescent state [8,9]. As a result, most current cancer therapies are able to produce short-term tumor remission, but they fail to prevent cancer relapse or metastasis.

More recently, cucurbitacins is a type of triterpenoids that are found to possess anti-cancer activity in additions to other pharmacological properties [10]. There are twelve known cucurbitacin types, with the B and E types being the primary and most-studied cucurbitacins [11,12]. A well-established cellular mechanism of cucurbitacins is that the compounds cause disruption of the F-actin cytoskeleton [13,14]. Cucurbitacins also interfere indirectly with microtubules polymerization [14]. Consequently, cucurbitacins were found to cause cell-cycle arrest at the G2/M phase [15]. Studies also identified many indirect intracellular targets, including the JAK2/STAT2 pathway, cofilin, cyclins [12]. While these findings nicely demonstrated the anticancer properties of cucurbitacins, concerns remain about whether or not cucurbitacins would be a good choice for cancer therapy, due to their lack of specificity for cancer cells.

Here, we present a project that began testing random herbal extracts for anticancer activity using melanoma and breast cancer cells. Two positive herbal extracts were identified. Through a series of chemical fractionation and biological tests for one of the positive extracts, we purified and determined cucurbitacin B as the anticancer compound. We showed that cucurbitacin B had a profound impact on the actin cytoskeletal system. More importantly, further studies using highly metastatic human melanoma and breast cancer cells showed that cucurbitacin B significantly inhibits cancer-cell invasiveness by reducing the cancer stem-cell population. Molecular studies found that cucurbitacin B also caused a decrease in the expression of stemness genes and an increase in the expression of anti-metastasis genes, making it a potential drug for preventing cancer metastasis. In addition, using zebrafish embryo as a vertebrate system for a toxicology study, we report the possible toxicity of cucurbitacin B, which appears to be primarily on the skin cells and a small subset of neurons.

2. Results

2.1. Anticancer Activity of Compounds in Bottle Gourd

To search for potential compounds with anticancer activity, we extracted natural compounds from plants. Different parts of the plants were dissected out, dried, and soaked in different organic solvent, such as methanol, ethanol, ethyl acetate, and hexane. This project focused on compounds extracted from bottle gourd (*Lagenaria siceraria*) grown in the Nanto and Taichung cities in Taiwan. We obtained 21 crude extracts containing compounds from the seed, placenta (tissue between seeds), flesh, or peel. The crude extracts were first tested on mouse melanoma cell B16F10 and on human breast-cancer cell MCF7, using the standard MTT cell-proliferation assay. The results showed that HLS3, HLS10, and HLS11 crude extracts consistently inhibited the proliferation of both cancer cell types
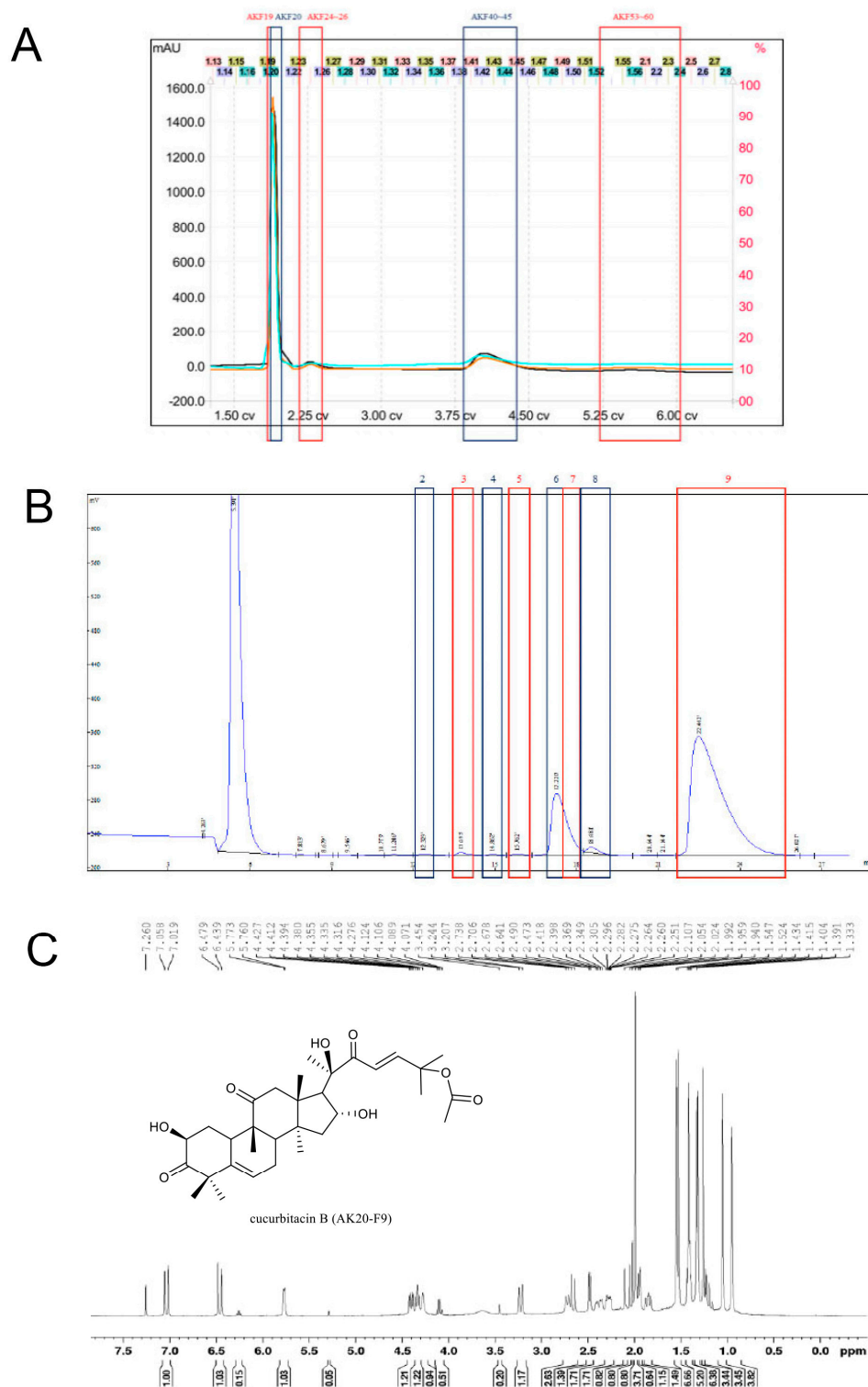
by approximately 50% (Figure 1A,B). These crude extracts are compounds extracted by methanol from the placenta (HLS3), peels (HLS10), and flesh (HLS11). HLS3 was chosen for further study, as it showed the strongest inhibition among the three positives. The compounds in HLS3 were separated by medium-pressure column chromatography (MPLC) with gradient methanol into ten fractions, named AK1 to AK10. These fractions were tested on cancer cells again and several fractions, AK8-AK10, showed strong inhibition (Figure 1C,D).
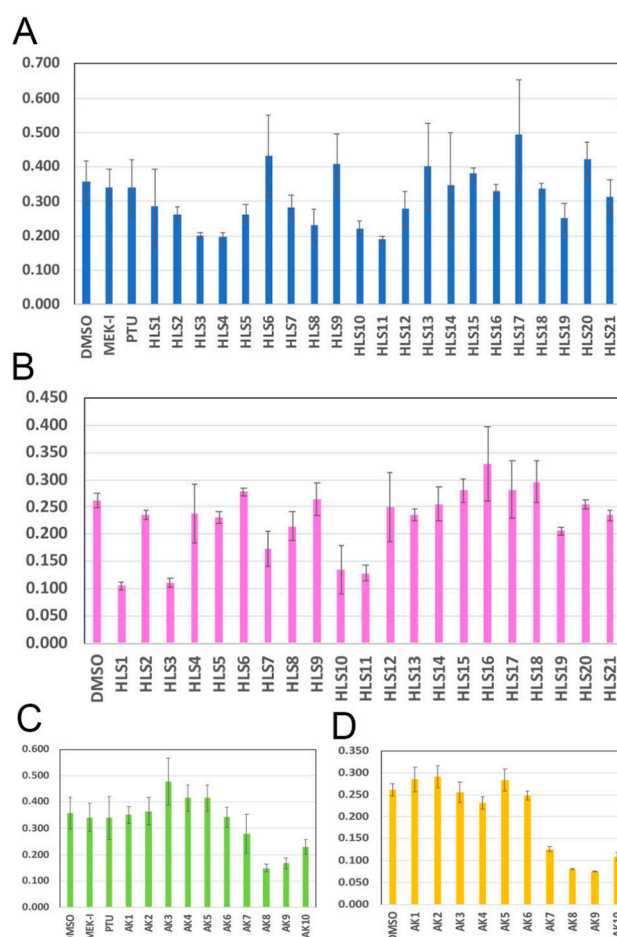

Figure 1. Crude extracts from bottle gourd showed anticancer activity. Twenty-one crude extracts containing compounds from different parts of bottle gourd were tested for the anticancer activity using the MTT cell proliferation assay. (**A**) In the mouse melanoma cell B16F10, the HLS3, HLS4, HLS10, and HLS11 crude extracts showed strong inhibition. Several negative controls were set up for comparison: DMSO, control solvent; MEK-I, inhibitor of MEK; PTU, phenyl thiourea. (**B**) In the human breast cancer cell MCF7, we observed consistent inhibition by HLS3, HLS10, and HLS11 crude extracts. (**C,D**) The HLS3 crude extract was separated by MPLC into ten subfractions, named AK1 to AK10. When these subfractions were tested again using the MTT assay, the AK8, AK9, and AK10 subfractions showed strong anticancer activity in both lung cancer (**C**) and prostate cancer (**D**). They also had strong inhibition strength on B16F10 and MCF7 cells.

A second run of MPLC was conducted to separate the compounds in the AK8-AK10 fractions. The eluent was separated into 65 test tubes, but the UV absorbance graph showed only five major groups of compounds (Figure 2A). The eluent within the same UV peak was combined to give us five major subfractions, named AK19, AK20, AK24-26, AK40-45, and AK53-60. The MTT assay was performed to show that the AK19, AK20, and AK24-26 subfractions strongly inhibited mouse melanoma-cell proliferation but the AK40-45 and AK 53-60 subfractions did not (Figure 3A). Interestingly, these positive subfractions showed

almost identical inhibition strength on several human cancer cell lines, including lung cancer (Figure 3B), prostate cancer (Figure 3C), melanoma, and metastatic breast cancer. Among the three positive subfractions, AK20 showed the largest peak on the UV graph (Figure 2A) and was chosen for further study.

Figure 2. Chemical purification and characterization of cucurbitacin B. (**A**) The positive AK8, AK9, and AK10 subfractions were combined and subjected to another MPLC separation. The UV absorbance of the eluent that was collected into 65 tubes indicated five major groups of compounds: AK19, AK20, AK24-26, AK40-45, and AK53-60 (top of the graph). (**B**) HPCL analysis for AK20 showed

eight major compounds, peaks #2–#9. (Peak #1 is the solvent.). The eluent was carefully separated into eight final fractions, AK20-F2 to AK20-F9. (**C**) The ¹H-NMR graph of AK20-F9 revealed a triterpene-like structure. Additional chemical characterizations confirmed AK20-F9 to be cucurbitacin B (Supplementary Figure S2).
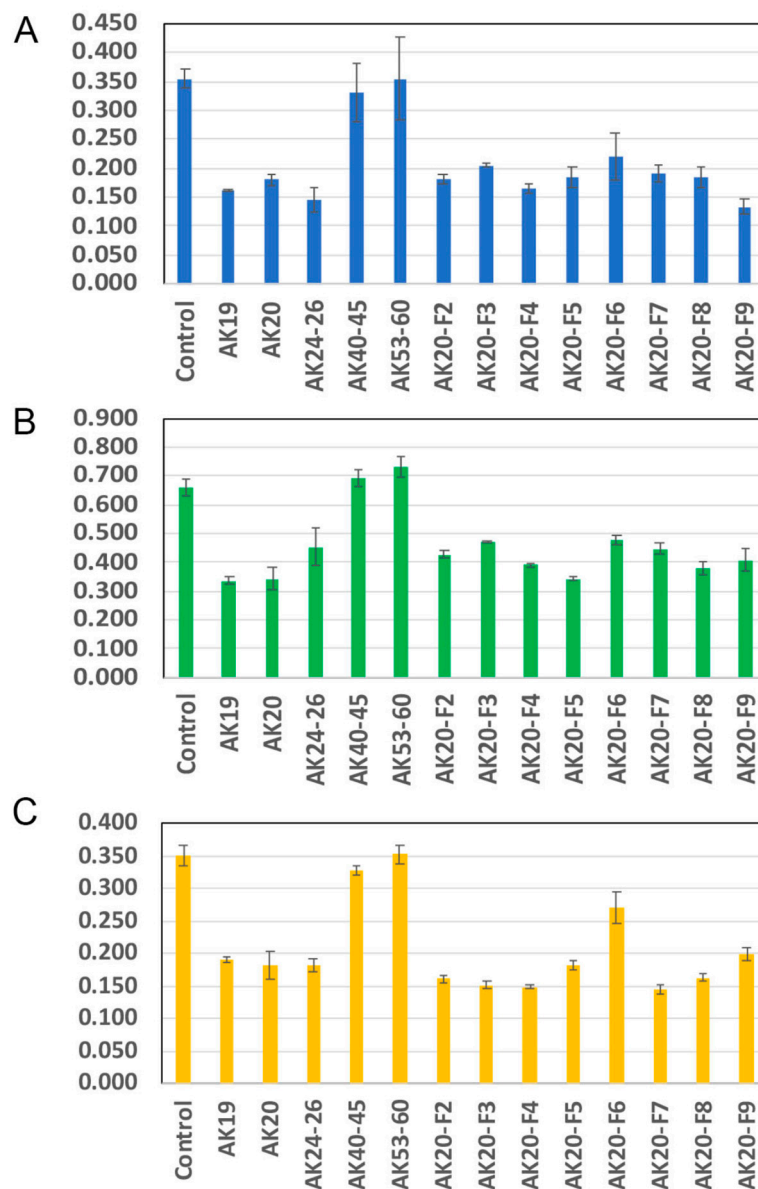
Figure 3. Proliferation inhibition of cucurbitacin B on various cancers. MTT assays for the subfractions and final fractions of bottle gourd compounds. The partially purified subfractions AK8, AK9, and AK10 were combined and separated by MPLC into the AK19, AK20, AK24-26, AK40-45, and AK53-60 subfractions. Among these five subfractions, AK19, AK20, and AK24-26 showed strong inhibition in B16F10 mouse melanoma cells (**A**), human non-small lung-cancer cells (**B**), and prostate-cancer cells (**C**). Left half of each graph. The compounds in the largest subfraction, AK20, were further separated by HPLC into eight final fractions, AK20-F2 to AK20-F9. Surprisingly, all the final fractions showed strong anticancer activity in mouse melanoma (**A**) and in human lung cancer (**B**). For prostate cancer, all the final fractions, except for AK20-F6, also showed strong inhibition (**C**).

Next, the compounds in AK20 were separated by high performance liquid chromatography (HPLC) using a hexane:ethyl acetate (55:45) solvent. Based on the UV absorbance, eight possible compounds were found (Figure 2B). They were carefully collected and named AK20-F2 to AK20-F9. The AK20-F1 compound was considered the solvent and, thus, it was

discarded. Since the AK20-F9 peak was well separated from others, it was predicted to be a pure compound. Several spectroscopic analyses were conducted to determine the structure of AK20-F9. The ^{1}H NMR spectrum showed nine methyl signals at δ_H 0.96 (3H, s, H-18), 1.03 (3H, s, H-19), 1.42 (3H, s, H-21), 1.53 (3H, s, H-26), 1.55 (3H, s, H-27), 1.33 (3H, s, H-28), 1.27 (3H, s, H-29), 1.34 (3H, s, H-30), and 1.95 (3H, s, OCOC<u>H</u>$_3$). In conjunction with the 32 signals observed in the ^{13}C NMR spectrum, AK20-F9 was found to be a cucurbitacin-type of triterpene. Using DEPT spectroscopy, we found that the NMR signals were due to nine methyl, four methylene, eight methane, and 11 quaternary carbons. Infrared (IR) spectrum showed the characteristic absorptions of the hydroxyl and conjugated carbonyl groups. ESI-MS data revealed the molecular weight of AK20-F9 to be around 558 g/mole and the molecular formula to be $C_{32}H_{46}O_8$. Finally, detailed analyses of HSQC, HMBC, and NOESY spectra helped us to perfectly match our NMR data with the reported structure of cucurbitacin B (Figure 2C and Supplementary Figure S2, [16]). The attempt to decipher the structure of compounds in other AK20 fractions proved to be difficult, as they were not pure enough. However, the NMR graphs indicated that they all contained a triterpene structure, which is the backbone of cucurbitacin. Thus, it was very likely that the AK20-F2 to AK20-F8 compounds contained other cucurbitacins (Supplementary Figure S1). Surprisingly, all the fractions of AK20 showed cell-proliferation-inhibition activity, ranging from 30% to 60%, in different cancer cells (Figure 3). Since AK20-F9 is a much more pure compound than other AK20 fractions, we conducted the rest of the study using AK20-F9 (hereinafter called cucurbitacin B).
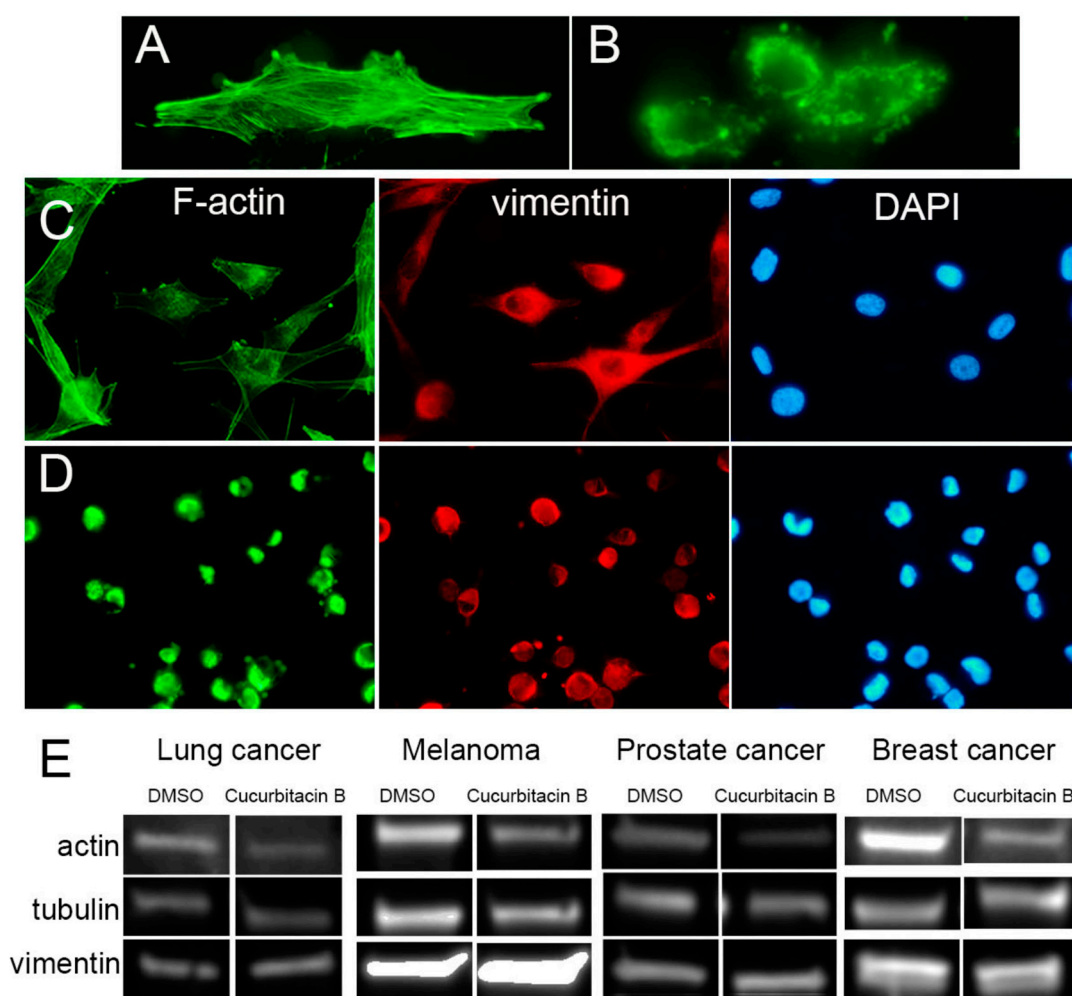
2.2. Cucurbitacin B Causes Cancer-Cell Retraction and Aggregation

During the MTT assays, we constantly observed striking morphological and behavioral phenotypes in cancer cells caused by cucurbitacin B, including the retraction of cellular processes, the roundup of cell shape, and aggregation. Interestingly, while melanoma cells tended to form small clusters of only two to four cells (Figure 4B), MCF7 breast-cancer cells formed much larger aggregates, with hundreds of cells (Figure 4D), but lung-cancer cells formed mostly small but occasionally medium aggregates (Figure 4F). Importantly, cucurbitacin B had much less effect on both the morphology and proliferation in a non-cancerous embryonic myoblast cell line (Figure 4H,I), compared with the strong inhibition on prostate-cancer cells (Figure 4J), suggesting that cucurbitacin B somehow poses stronger toxicity on cancer cells.

The dramatic cell-shape changes indicated the strong effect of cucurbitacin B on the actin cytoskeletal structures. As reported by other groups [13,14], we observed near total collapse of the actin filaments using the FITC-conjugated phalloidin (Figure 5B). Our attempt to study the effect of cucurbitacin B on intermediate filament and microtubule systems appeared uninformative. Immunostaining using an anti-vimentin antibody showed aggregates of intermediate filaments in cucurbitacin B-treated cells (Figure 5D), which we believe is a secondary effect of cell retraction. To confirm the selective effect of cucurbitacin B on the actin cytoskeletal system, we performed a Western blot experiment. Indeed, cucurbitacin B caused a significant reduction in β-actin protein but had little or no effect on vimentin, tubulin (Figure 5E), or keratin 17 and 19.
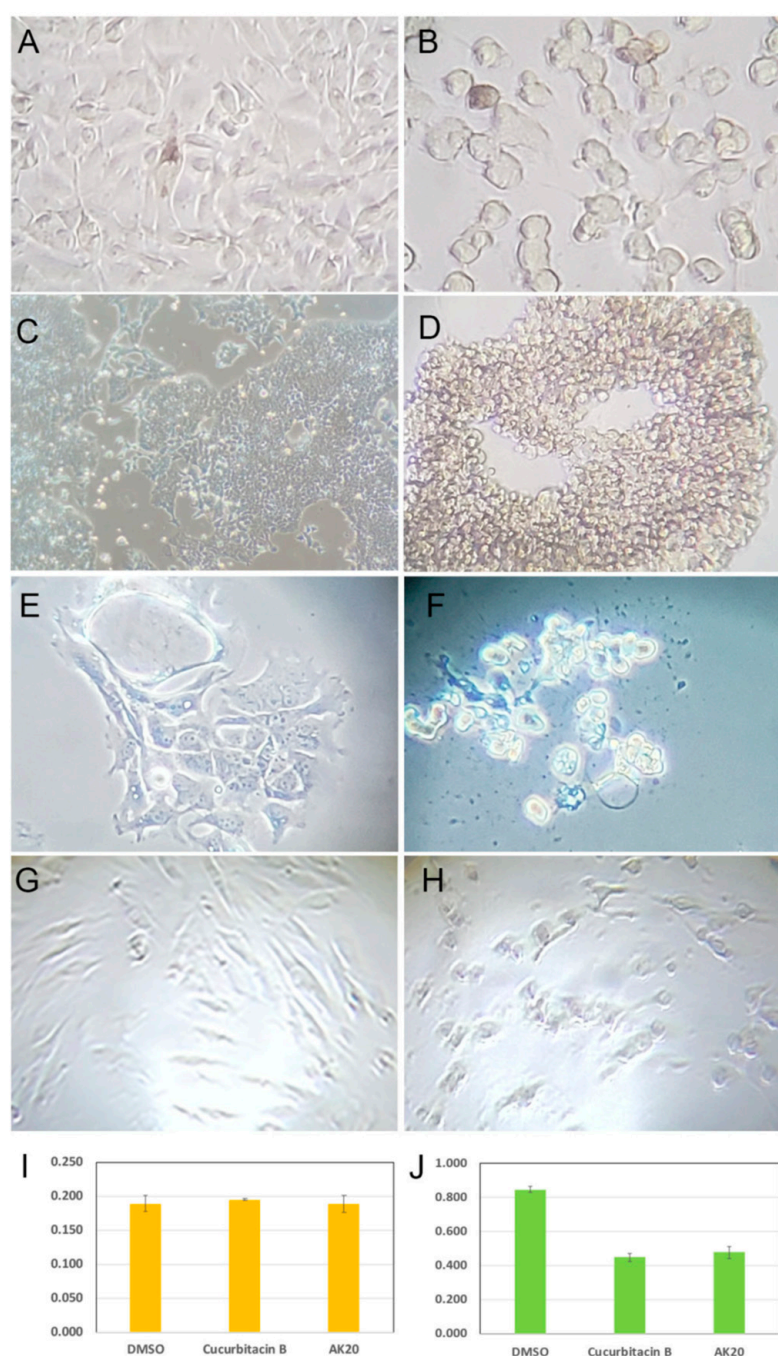
Figure 4. Cucurbitacin causes changes in cell shape and behaviors. (**A,B**) B16F10 mouse melanoma cells in DMSO control solvent show normal fibroblast morphology (**A**) but retract to round shape and form small aggregates in cucurbitacin B (**B**). (**C,D**) Cucurbitacin B causes large aggregates in MCF7 breast-cancer cells (**D**). (**E,F**) In non-small lung-cancer cells, cucurbitacin B also causes cell retraction and aggregation. (**E**), DMSO; (**F**), cucurbitacin B. (**G,H**) The rat myoblasts CRL1446 show the characteristic spindle shape in DMSO (**G**) and only slight retraction in cucurbitacin B (**H**). (**I,J**) MTT experiments show that cucurbitacin B has no effect in myoblast cells (**I**) but strong inhibition on prostate-cancer cells (**J**). AK20 is the partially purified extract that contains cucurbitacin B.

Figure 5. Cucurbitacin B causes collapse of F-actin and reduction of b-actin protein in cancer cells. (**A**,**B**) B16F10 mouse melanoma cells were treated with DMSO control solvent (**A**) or cucurbitacin B (**B**), fixed with 4% PFA, and stained with FITC-conjugated phalloidin. The F-actin (filamentous actin) network was well-extended and organized in the control cells but appeared collapsed in the cucurbitacin B-treated cells. (**C**,**D**) Human melanoma cells COLO829 were used to examine the effect of cucurbitacin B on the actin system using the FITC-conjugated phalloidin (green), as well as the intermediate filament using the anti-vimentin antibody (red). The cells were also counter stained with DPAI for the nuclei (blue). (**E**) Western blot revealed that cucurbitacin B in fact significantly reduced the amount of β-actin in lung-, melanoma-, prostate-, and breast-cancer cells. Cucurbitacin B, however, had little or no effect on the amount of tubulin and vimentin, except in melanoma cells. Note that the two bands in the vimentin panel of breast cancer actually contain vimentin (upper band) and keratin 17 (lower band), which are both components of intermediate filament and appear in about the same amount between the control and cucurbitacin B-treated cells.

2.3. Cucurbitacin B Reduces Cancer-Cell Invasiveness and Cancer Stem Cells

The cancer-cell roundup and clustering might lead to two seemingly opposite consequences for the cells. On one hand, the cancer cells became smaller and less bound to each other, a morphological similarity to cancer stem cells, allowing them to be more invasive. On the other hand, the collapse of actin filament might impair the migration ability and reduce cell invasiveness. To distinguish these two hypotheses, we adopted an in vitro cell invasion assay that utilized a collagen-coated membrane to mimic the extracellular matrix barrier between cancer cells and stromal cells. The cancer cells were prepared on the collagen with a serum-free medium and/or cucurbitacin B. On the other side of the membrane, a serum-containing medium was set up to attract invasive cancer cells to penetrate the

collagen layer. After 24-h incubation, the cancer cells that appeared on the non-collagen side of the membrane were stained, followed by a cell count and spectrophotometric measurement of the cell lysate (see the Section 4 for details). For this experiment, we used the highly invasive human breast-cancer cell MDA-MB-231 and melanoma cell COLO829. As predicted, we observed a slight decrease in the invasiveness in the MDA-MB-231 cells by cucurbitacin B (Figure 6B). When culturing human melanoma cell COLO829, we noticed a significant amount, around 30%, of cells floating in the medium (unpublished data). These floating cells were alive and, when transferred to a new flask, able to reestablish a new population of adhering and floating cells. Similarly, when adhering cells were trypsinized and transferred to a new flask, a similar percentage of floating cells appeared. We suspected that the different behaviors may have been associated with different degrees of invasiveness and, therefore, performed the invasion assay with the two types of melanoma cells separately. As was the case with breast-cancer cells, we first observed a slight decrease in the invasiveness by cucurbitacin B in adhering melanoma cells (Figure 6D). When floating melanoma cells were used, we observed a significant decrease in invasiveness by cucurbitacin B (Figure 6E,F).
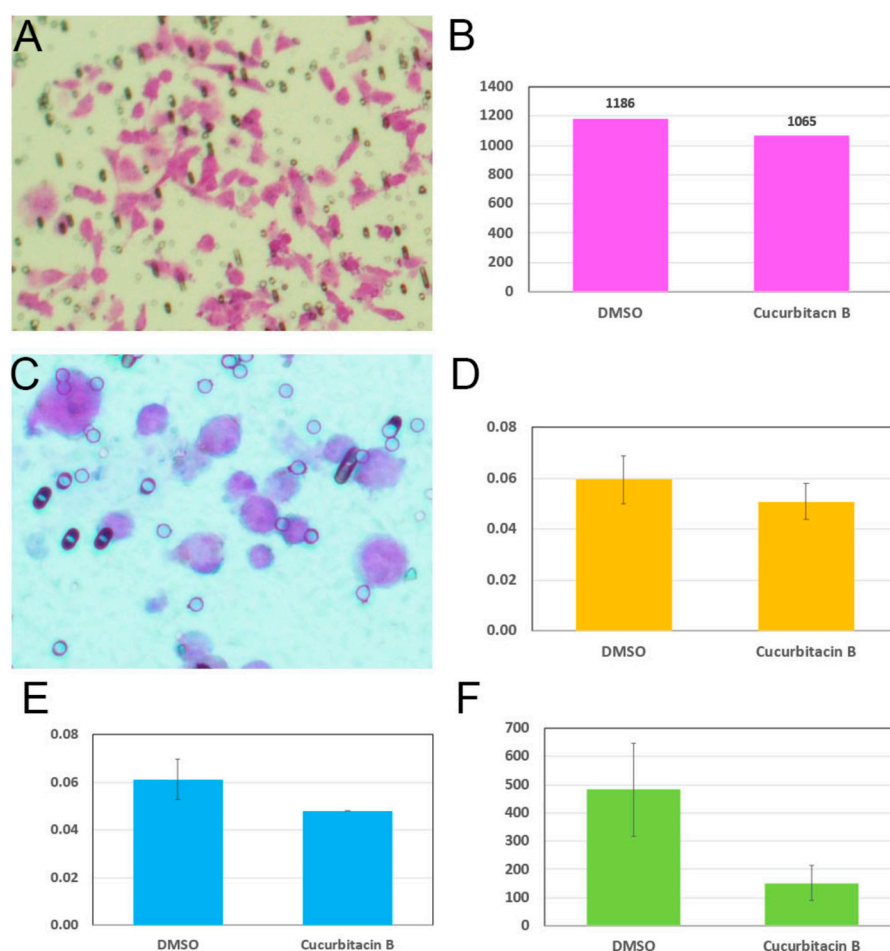
Figure 6. Cucurbitacin B reduces the invasiveness in highly metastatic breast and melanoma cancer cells. An in vivo cell invasive assay was performed to evaluate the cancer-cell invasiveness. (**A**) The stained invasive MDA-MB-231 breast-cancer cells that penetrated the collagen layer. (**B**) Cell counts of invasive breast cancer in DMSO control and cucurbitacin B. ($n = 1{,}500{,}000$ cells per group). (**C**) Stained human melanoma cells migrated across the collagen layer. (**D**) Cell-invasion assay result with adhering human melanoma cells. Note that the graph is based on the absorbance of the homogenized stained cells at 560 nm. (**E**,**F**) Cell-invasion assay result with floating human melanoma cells, analyzed by spectrophotometry at 560 nm (**E**) or cell count (**F**). ($n = 600{,}000$ cells per group).

It is widely accepted that cancer stem cells are responsible for the invasiveness and metastasis of cancers. We tested whether cucurbitacin B has any effect on cancer stem cells. To do this, immunostaining experiments to label cancer stem cells were performed on cancer cells with or without cucurbitacin B. For this experiment, we chose human melanoma COLO829 cells because of their well-characterized stem cell markers, CD133 and CD271 [17,18]. The cells were prepared on silicon-coated slides and treated with cucurbitacin B for 24 h, followed by immunostaining with FITC-conjugated anti-CD133 and PE-conjugated anti-CD271 antibodies. The number of double-labeled cells were counted with an epi-fluorescence microscope. We chose to manually count the labeled cells simply because there was no working flow cytometer available in our institution. After examining approximately 500,000 cells for each treatment group, cucurbitacin B clearly showed a significant reduction in melanoma stem cells (Figure 7A). When the percentage of melanoma stem cells was calculated, we observed 0.165% stem cells in the control melanoma COLO829 but only 0.05% in the cucurbitacin B-treated COLO829 (Figure 7B).
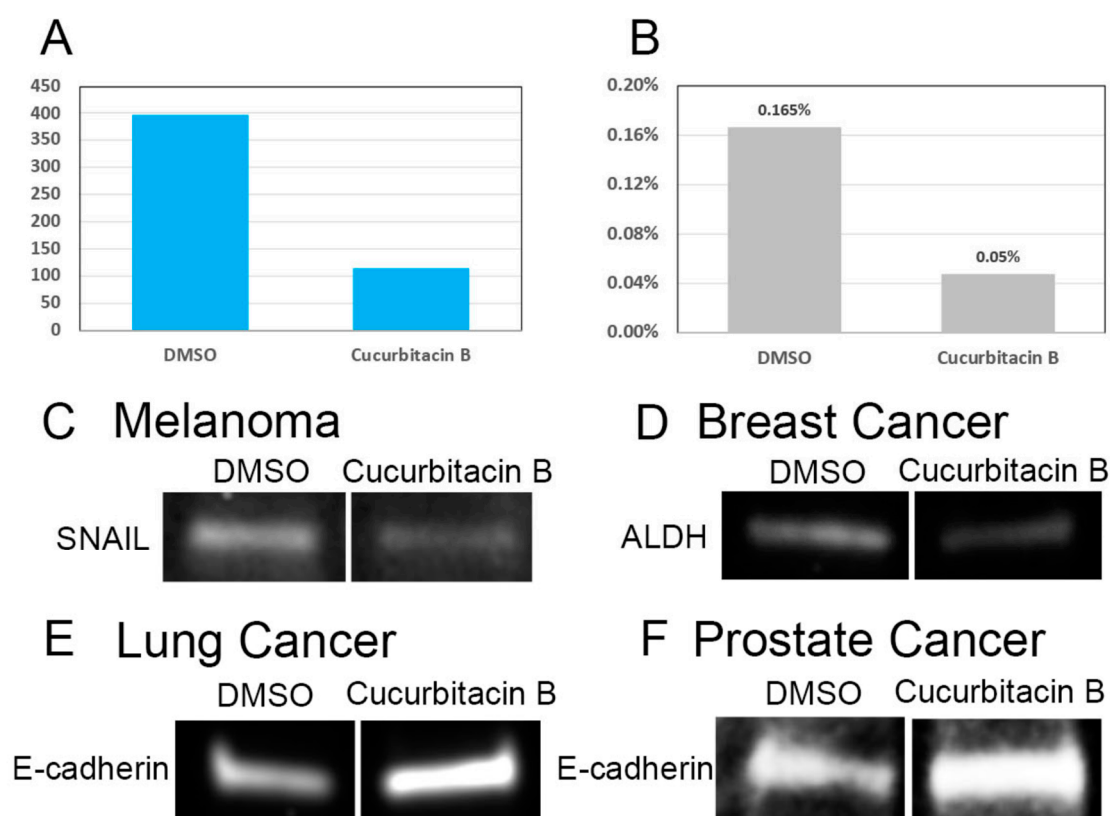
Figure 7. Cucurbitacin B reduces melanoma stem cells. (**A**,**B**) The highly metastatic human melanoma cells COLO829 were incubated in control solvent DMSO or 10 μM of cucurbitacin B for 24 h, followed by immunostaining using FITC-conjugated anti-CD133 and PI-conjugated anti-271 antibodies. The cells were analyzed under a fluorescence microscope and the double-stained cells were counted. (**A**) Cell-count graph showed a significant decrease in the melanoma stem cells by cucurbitacin B. ($n > 500,000$). (**B**) The percentage of melanoma stem cells. (**C**) Western blot experiments showed a decrease in the metastasis-promoting transcription factor SNAIL in cucurbitacin-treated melanoma cells. (**D**) Cucurbitacin B also causes a decrease in the known marker ALDH1A1 (aldehyde dehydrogenase 1 A1) for breast-cancer stem cells. (**E**,**F**) Cucurbitacin B caused an increase in the metastasis-inhibiting protein E-cadherin in cucurbitacin-treated lung and prostate-cancer cells.

To obtain supporting molecular evidence, we performed a Western blot experiment to examine the metastasis-associated proteins. For this experiment, we used several different cancer cells to determine whether the same molecular effect by cucurbitacin B could be

obtained. We first observed a decrease in the known metastasis-promoting transcription factor Snail in cucurbitacin B-treated human melanoma COLO829 cells (Figure 7C), supporting the reduction in invasiveness and in the cancer stem cells described above. The epithelial marker E-cadherin, which is known to be associated with reduced cell invasiveness, was increased in cucurbitacin B-treated lung and prostate-cancer cells (Figure 7E,F). E-cadherin appeared to express at very low level in COLO829 and MDA-MB-231 cells, causing difficulties in data interpretation.
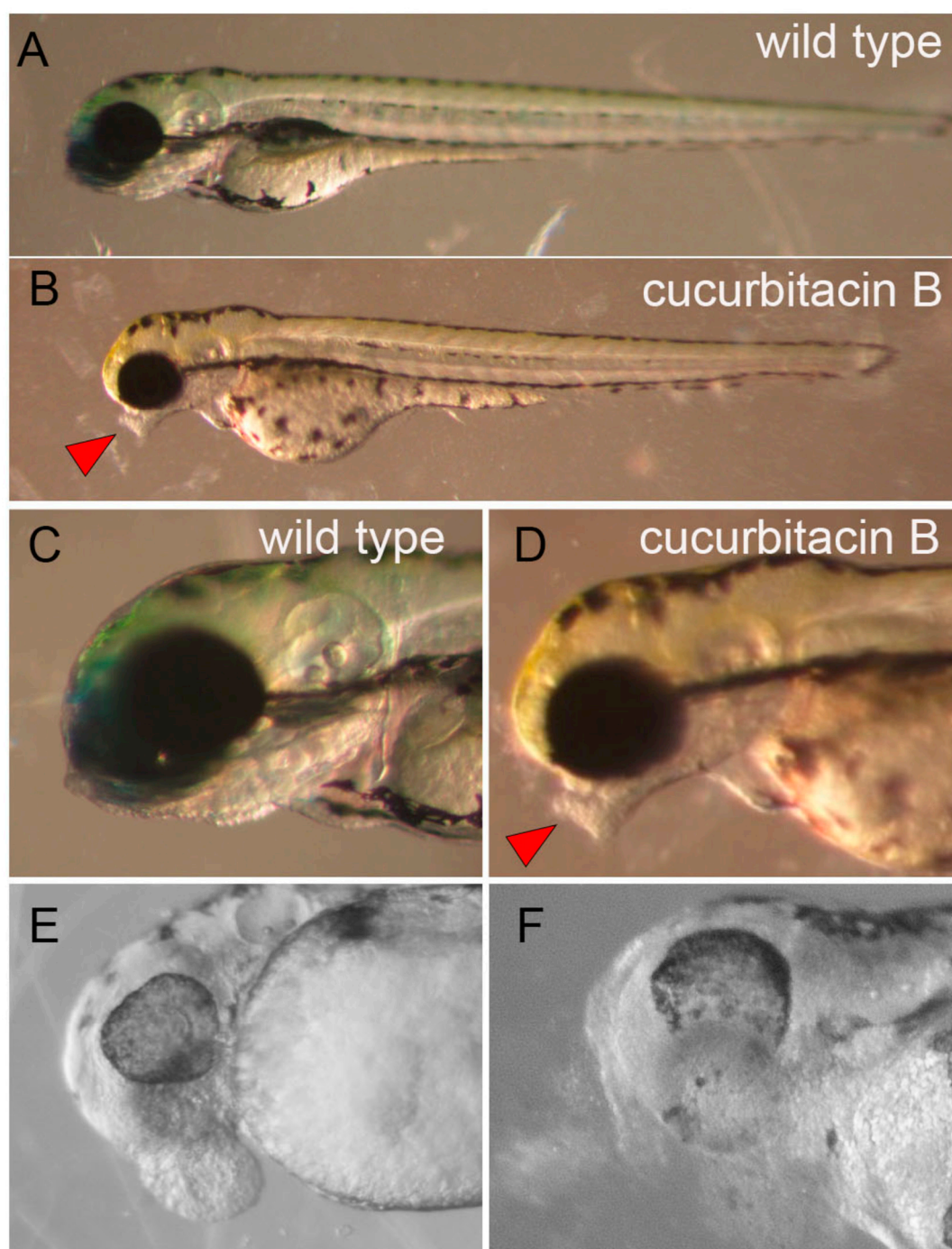
2.4. Cucurbitacin B Toxicity on Developing an Olfactory Organ in Zebrafish Embryo

Finally, we tested whether cucurbitacin B has any toxicity on developing embryos, using zebrafish. We hypothesized that cucurbitacin B would halt the epiboly movement of early embryogenesis, which heavily utilizes the actin cytoskeletal system and starts at around 4h post-fertilization (hpf). To our surprise, zebrafish embryos incubated in cucurbitacin B from 4–24 hpf showed no morphological defect at all. The epiboly cell movement occurred normally. Embryos that were incubated with cucurbitacin B from 24–48 hpf, however, developed bumps that often appeared near the mouth, sometimes in the head, and rarely in other locations (Figure 8). The tolerable toxicity concentration of cucurbitacin B was very narrow, with 0%, 50%, and nearly 100% of the embryos developing the bump phenotypes by 4, 8, and 10 μM cucurbitacin B, respectively. Unfortunately, 10 μM cucurbitacin B also caused ~40% mortality within 24 h of incubation and 60–70% mortality after 48 h. The dead embryos typically showed severe tissue degradation starting in the head, while the trunk appeared morphologically intact (Figure 8F). Immunostaining using antibodies for various tissues showed that the head bumps were not composed of neurons or muscle cells (data not shown). The cells in the bump expressed tight junction proteins revealed by the ZO-1 antibody (Supplementary Figure S3), indicating that they were likely skin cells. An anti-acetylated tubulin antibody that primarily labeled the surface neurons throughout the body, including the lateral line [19], however, revealed that the bumps were innervated (Figure 9B). While the surface sensory system in the trunk appeared to be normal (Supplementary Figure S3), the surface neuronal network in the head showed several prominent abnormalities, including the missing or poorly formed neuronal network of the olfactory organ in the nostrils (Figure 9D) and an unstructured network above the eyes (Figure 9F).

3. Discussion

3.1. Cucurbitacin B for Cancer Metastasis Treatment

In addition to the same cellular phenotypes observed by other groups, our study further showed that cucurbitacin B can reduce cancer-cell invasiveness. Our results are convincing, as the same effect was observed in the highly metastatic breast-cancer and melanoma cells (Figure 6). We further showed that the reduction in invasiveness was associated with the reduced number of cancer stem cells (Figure 7). Although in a manual approach, the data presented in Figure 7 appeared unequivocal, as the sample size was large (more than 500,000 cells) and the calculated stem-cell percentage perfectly fell into the reported CSC range of 0.1% to 0.0001% [3,20,21]. Our attempt to quantify the cancer stem cells in breast cancer, unfortunately, turned out to be fruitless, because the cells did not adhere well to the silicone-coated slide. Nevertheless, our Western blot experiment with melanoma and breast cancer showed consistently supporting results, with reduced expression of pro-metastasic and stemness genes (Figure 7). All these results strongly suggest that cucurbitacin B indeed can reduce the number of cancer stem cells at least in melanoma and in the triple-negative breast cancer from which the MDA-MB-231 cells are derived. We suspect that cucurbitacin B would have the same effect on other cancers as well. Our evidence, although strong, is not comprehensive. Further studies using an in vivo cell-invasion system, more cancer stem cell markers, and more molecular characterization are needed. Once proved, cucurbitacin B could be a compound to reduce the probability of cancer relapse and metastasis.

Figure 8. Cucurbitacin B toxicity in developing zebrafish embryo. To test whether cucurbitacin poses any toxicity to developing embryos, we incubated zebrafish embryos with cucurbitacin B between 4–72 h post fertilization (hpf). Shown are 72-hpf embryos. (**A**,**B**) Whole embryo views and (**C**,**D**) closeup views of the heads of (**A**,**B**) show that cucurbitacin B caused a mild morphological phenotype, with a small bump in the head (red arrowhead in (**B**,**D**)), while the rest of the body appeared normal. (**E**) The bump phenotype could be more severe and was mostly in the head. (**F**) Higher concentration (10 μM) or prolonged incubation of cucurbitacin B could eventually cause mortality in the embryos, starting with tissue degradation in the head.
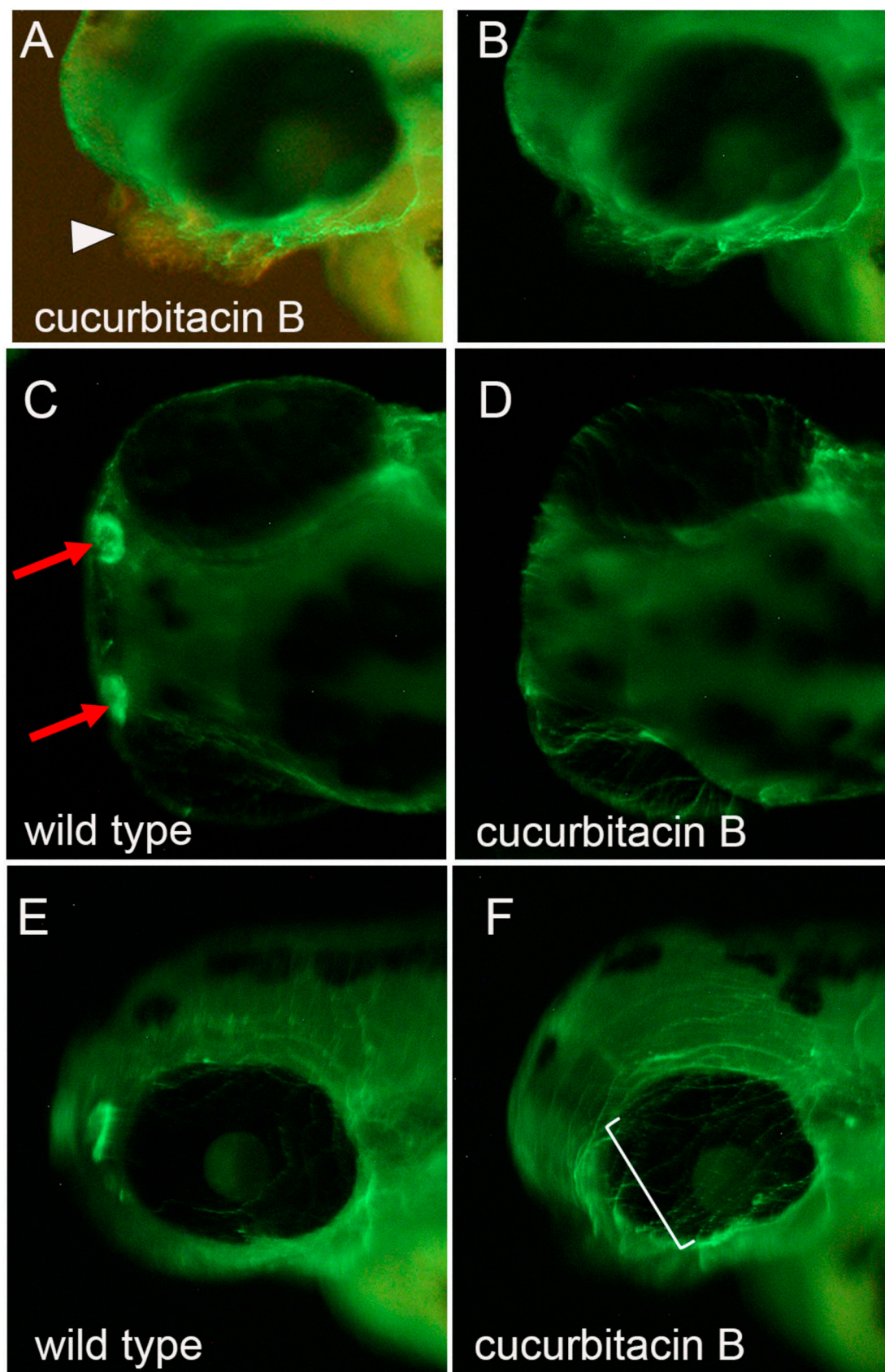
Figure 9. Cucurbitacin B toxicity in developing embryo. Immunostaining using anti-acetylated tubulin antibody revealed defects in the developing surface sensory nervous system caused by cucurbitacin B.

Images here are an anterior view of 72 hpf zebrafish embryos. (**A**,**B**) The same cucurbitacin B-incubated embryo showed the typical bump phenotype in the head (arrowhead in (**A**)) which is innervated by surface neurons revealed by the Alexa-488 conjugated anti-acetylated tubulin antibody (green). (**C**,**D**) The olfactory organ in the two nostrils are brightly stained in the wild type embryo (red arrows in (**C**)) but missing in the cucurbitacin B-incubated embryo (**D**). (**E**,**F**) The surface neurons above the eyes appears parallel and unstructured in the cucurbitacin B-incubated embryo (bracket in (**F**)), compared with the more structured surface neurons in the wild type (**E**).

3.2. Cytoskeletal Restructuring and Stem-Cell Behaviors

The most profound cellular toxicity of cucurbitacin B is the disruption of the filamentous actin system [12,14]. In addition to the actin phenotype, we also observed a cell-aggregation phenotype, suggesting alteration of the cell-adhesion molecules and the property between cells. We noticed that these cells, while partially losing attachment to the culture dish, were not dead, as was evident from the MTT staining. Another interesting observation was that the aggregation phenotype differed in different cancer cells, suggesting the differential molecular effect of cucurbitacin B on cancer-cell adhesion. In a review article by Farahani et al. in 2014, a current model for metastasis started with the establishment of the so-called pre-metastatic niche, which seemed to be largely dependent on the cell-adhesion molecules. It will be interesting to examine how and what cucurbitacin B alters in the cell-adhesion molecule profiles in different cancers.

3.3. Differences between Cucurbitacins and Other Cytoskeleton-Targeting Compounds

Unlike paclitaxel and vinblastine, which inhibit microtubule polymerization and, consequently, mitosis, cucurbitacin B causes the depolymerization of actin and secondarily defects in microtubule polymerization [14]. Although the disruption of actin and microtubule by cucurbitacin B can explain cell-cycle arrest, our results provide insight into the different modes of action and the potential uses between cucurbitacin B and other cytoskeleton targeting drugs for cancer therapy. First, cucurbitacin B had no effect on the proliferation of the embryonic myoblasts, even though the treated cells still showed some degree of retraction (Figure 4). This result strongly suggests that cucurbitacin B has some kind of selectivity toward cancer cells over non-cancerous cells. It is likely that cucurbitacin B disrupts multiple cell-adhesion molecules, some of which are in non-cancerous cells and not involved in cell proliferation, but others that are expressed in cancer cells that are responsible for regulating the stemness and invasiveness of cancer-cell behaviors. As most of the CSC markers identified to date are actually cell-adhesion molecules [22], our findings suggest a possibility that cucurbitacin B might target the CSC-adhesion molecules to cause losses in the stemness and invasiveness of CSCs.

3.4. Cucurbitacin Toxicity in Developing Embryo

With the strong toxicity of cucurbitacin B on the filamentous actin system in cancer cells, we expected to see a catastrophic effect of cucurbitacin B on developing embryos, as active cell movement is one of the essential cellular functions for embryogenesis. To our big surprise, cucurbitacin B had no effect during gastrulation when active cell movement formed the three germ layers. In particular, it is well documented that the actin and microtubule systems are required for epiboly movement during early gastrulation [23]. In the cucurbitacin B-treated zebrafish embryo, epiboly movement occurred normally, indicating that cucurbitacin B toxicity was not targeting the cytoskeletal system. We did not observe any phenotype caused by cucurbitacin B until around 48 h post fertilization. The phenotype, which was much milder than expected, appeared as a bump in the head surface (Figure 8). The embryos were able to grow to normal size with grossly normal morphology. Based on the characterizations we made, the bump was likely to have been composed of skin cells that could be properly innervated by surface neurons. Follow-up observations revealed that the bump could become deteriorated, causing the disintegration of tissue from the head and, eventually, death. These observations suggested to us that

the root problem in the bump formation is tissue disintegration, and death is likely due to cell-adhesion defects.

The zebrafish olfactory system contains ciliated neurons [24] and, thus, it is stained brightly by the anti-acetylated tubulin antibody (Figure 9C; [25]). The absence of ciliated neurons in the nostril, caused by cucurbitacin B, suggests that perhaps cucurbitacin B has a direct impact on neuronal differentiation and/or axon pathfinding, possibly through the actin filament and/or microtubule systems. This notion is supported by the unstructured axons above the eyes. However, we did not observe a similar phenotype in the lateral line or in nearly all the surface neurons in the trunk (Supplementary Figure S3), suggesting that cucurbitacin B toxicity is somewhat tissue-specific. This specificity is likely due to the unique molecular receptor(s) expressed on the affected tissues. It will be interesting to identify the cucurbitacin B receptor(s) to understand which tissues or cell types are more vulnerable to cucurbitacin B toxicity.

4. Materials and Methods

4.1. Chemical Extraction and Isolation

Bottle gourd (*Lagenaria siceraria*) were purchased from the local market in the Nanto and Taichung cities of central Taiwan. Different parts of the fruit were dissected out, dried, and ground into powder. Approximately 200 g of each part were soaked twice in 95% ethanol with ultrasound vibration for 30 min. The compounds were further separated into a polar group using ethyl acetate (EA) and a non-polar group using *n*-hexane, resulting in a total of 21 crude extracts (HLS1~HLS21) containing compounds from seed, placenta tissue, flesh, or peel. The positive crude extracts identified in our initial MTT assay (Figure 1) were HSL3 with EA-extracted compounds from the placenta tissue, HLS10 with EA-extracted compounds from the peels, and HLS11 with EA-extracted compounds from the flesh.

The HLS3 crude extract was further fractionated with a step gradient elution of methanol/water gradient from 100% to 0% on a C_{18}-gel column (330 g; 539 mL; particle size 40–63 mm; I.D. 60.6 × H187 mm, ILOK^{TM}) by MPLC into ten fractions (AK1 to AK10).

The positive AK8, AK9, and AK10 subfractions were combined and separated by another run of MPLC (120 g; 215 mL; particle size 40–63 μm; I.D. 36.6 × H204 mm, ILOK^{TM}), again with a methanol/water gradient, 100% to 10%. The eluent was collected into five subfractions: AK19, AK20, AK24-26, AK40-45, AK53-60 (Figure 2A). The numbers corresponded to the test tubes that collected the eluent. The AK20, which showed the highest UV absorbance and tested positive in the subsequent MTT assay, was selected for the next chemical separation by HPLC using hexane:ethyl acetate (55:45) solvent at a flow rate of 3.0 mL/min. The compounds were separated quite well (Figure 2B), resulting in eight near-pure compounds, AK20-F2 to AK20-F9. The AK20-F1 was the solvent and, thus, was discarded. The AK20-F9 ($_R$ = 22.4 min) was analyzed by ESIMS and 1D and 2D NMR and determined to be cucurbitacin B (Supplementary Figure S2). Due to impurities, the structure of other compounds was still not conclusive, but apparently contained triterpene (Supplementary Figure S1).

4.2. Cell Culture

All the cell lines used in this study were purchased from the American Tissue Culture Center (ATCC, Manassas, VA, USA), including the mouse melanoma cell line B16F10 (CRL-6475, DMEM with 10% FBS), human melanoma cell COLO829 (RPMI w 10% FBS), human triple negative breast-cancer cell MDA-MB-231 (DMEM w 10% FBS), human non-small lung-cancer cell HTB178 (RPMI w 10% FBS), human prostate-cancer cell DU145 (EMEM w 10% FBS), and rate embryonic myoblasts CRL1446 (DMEM w 10% FBS). Trypsinization and subculture were performed, following the protocols found on the ATCC website.

4.3. MTT Assay

A detailed MTT protocol was previously published by our lab [26]. For this project, an equal number of cancer cells, approximately 10,000–20,000 cells, were plated into

individual wells of a 96-well plate. After the cells reattached to the culture well, chemicals were administered at, typically, a 10 μM concentration, unless specified, and the cells were allowed to incubate for 24 h. The culture medium was then replaced with PBS containing the MTT substrate. The reaction was incubated for 30–60′, followed by the addition of an SDS—HCL solution to dissolve the purple formazan overnight. The dissolved formazan was analyzed with a microplate reader (Model 680, Bio-Rad, Foster City, CA, USA) at 570 nm.

4.4. Immunostaining with Cancer Cells

To detect the cancer stem cells, the cells were first seeded onto Teflon-coated well slides (HTC Super-cured, 4-well, Cell-Line/Thermo Fisher, Waltham, MA, USA) with 50 μL of growth medium. After 24 h of chemical treatment, the cells were fixed with 4% paraformaldehyde (PFA) for 24 h at 4 °C. The cells were then washed several times with PBS before being incubated with blocking buffer (3% BSA, 1% DMSO in PBS) for an hour at room temperature. After the blocking, primary antibodies were added and incubated overnight at 4 °C. The primary antibodies used were the CD133 monoclonal antibody (13A4), FITC (Thermo Fisher Scientific, Waltham, MA, USA, 1:100 dilution), the CD271 monoclonal antibody (ME20.4), PE (Thermo Fisher Scientific, Waltham, MA, USA, 1:100 dilution), and vimentin (D21H3) XP Rabbit mAb (Cell Signaling Technology, Danvers, MA, USA, 1:1000 dilution). For some experiments, the cells were washed and incubated with Alex594-conjugated goat-anti-rabbit IgG secondary antibody (Jackson ImmunoResearch Laboratories, Inc, West Grove, PA, USA, 1:1000 dilution) for two hours at room temperature, followed by several washes with PBS and/or FITC-conjugated phalloidin. Finally, a drop of ProLong Gold Antifade Reagent with DAPI (Cell Signaling Technology, Danvers, MA, USA) was applied to the stained cells. For the cancer stem cell experiment, ~40,000 human melanoma cells were seeded on each well of 13 slides. The number of CD133 and CD271 double-positive cells was manually counted and graphed.

4.5. Cell-Invasion Assay

For this experiment, the CHEMICON Cell Invasion Assay Kit was purchased from Millipore Sigma, St. Louis, MO, USA (Cat. No. ECM 550, 8 μM). The cells were prepared in a serum-free medium at a 10^6 cells/mL concentration and 300 μL of cells were seeded in each invasion chamber, 30,000 cells per chamber, with or without the compound. The invasion chambers with cells were placed in a 24-well plate with 0.5 mL of complete medium. The cells were allowed to migrate overnight. On the next day, the cells that remained in the invasion chamber were carefully cleaned using cotton swabs. The cells that penetrated the collagen and appeared on the lower surface of the polycarbonate membrane were stained with toluidine blue, followed by extensive washes with ddH2O. The membrane was then cut off and mounted on a slide. The stained cells were counted with a compound microscope or dissolved in 200 μL of 10% acetic acid. The cell lysate was transferred to a 96-well plate for colorimetric measurement at 560 nm using a microplate reader (Model 680, Bio-Rad, Foster City, CA, USA).

4.6. Western Blot

Typically, 320,000 cells were prepared in a 6-well plate, two wells per chemical, and allowed to grow for 24 h. Chemicals were added into each well at 10 μM and incubated for 24 h. To harvest the proteins, the medium was removed and the cells were briefly washed with PBS and scraped using a cell scraper with 200 μL of freshly prepared lysis buffer (0.2% NP-40, 100 mM Tris, 150 mM NaCl, 8 mM of EDTA, pH 7.4) with a protease inhibitor cocktail (P8340, Sigma, St. Louis, MO, USA). The cells were lysed in 1.5 mL microcentrifuge tubes overnight on a shaker at 4 °C. The lysate was then centrifuged at 12,000 rpm at 4 °C for 20 min. After the centrifugation, the protein supernatant was transferred to a clean tube and stored at −80 °C. Using the Pierce BCA Assay Kit (23227, Thermo Scientific, Waltham, MA, USA), the protein concentrations were analyzed. Ten to twenty μg of protein were loaded into a 12% SDS–PAGE gel (Biorad, Hercules, CA, USA) for gel electrophoresis. The

Western blotting was performed using the Pierce Fast Western Blot Kit (35050, Thermo Scientific, Waltham, MA, USA). Antibodies were purchased from Cell Signaling Technology, Danvers, MA, USA, including β-actin (Cat. No. 3700, 1:500), vimentin (Cat. No. 5741, 1:500), acetylated-α-tubulin (Cat. No. 5335, 1:1000), ALDH1A1 (Cat. No. 54135, 1:1000), E-cadherin (Cat. No. 14472, 1:1000), and Snail (Cat. No. 3879, 1:1000).

4.7. Zebrafish Husbandry and In Vitro Fertilization

Our lab has been using zebrafish for developmental biology and toxicology studies for years. An IACUC protocol was created following the "Guide for the Care and Use of Laboratory Animals" published by the NIH (NIH Publication No. 85-32, revised in 1985). The zebrafish stocks are maintained following standard procedures [27] and bred by in vitro fertilization. A detailed protocol may be found in Haege et al., 2021 [28]. In brief, after overnight incubation, adult zebrafish were anesthetized briefly and the eggs were collected in a petri dish by gently milking the female fish's belly. The sperm was collected from the male fish using a capillary tube. The sperm was mixed with the eggs in the petri dish. The fish were immediately placed back in regular water to allow for recovery. The fertilized embryos were placed in an incubator set at 28–30 °C.

4.8. Chemical Preparation for Zebrafish Experiments

In the early stages of the project, as the extracts were mixed with an unknown number of compounds, we assumed that the average molecular weight of these compounds was about 300 g/mole, measured the weight of dried extracts, and calculated the volume of DMSO to yield 100 mM of extracts. With the assumption that the active compounds with biological activity, if any, were likely to make up 10% of the extract, the 100 mM extract was expected to contain 10 mM of the active compound.

4.9. Chemical Treatment of Zebrafish Embryos

After a couple of hours of incubation, the zebrafish embryos were sorted (fertilized/unfertilized) and stained with Methyl Blue, then placed back into the incubator. Embryos with normal morphology of different stages were transferred into wells of a 96-well plate, each well having five embryos with approximately 200 μL of egg water (distilled water containing 60 μg/mL sea salt. The chemicals were diluted in egg water at 10 μM. The egg water was removed and 200 μL diluted chemical was added to the well. The embryos were then paced in a 28–30 °C incubator and examined daily.

4.10. Immunohistochemistry with Zebrafish Embryos

The embryos were deshelled and fixed in 4% paraformaldehyde at least overnight at 4 °C. The fixed embryos were washed twice with PBS, then once with H_2O, 5 min/each, and permeabilized with -20 °C acetone for 7 min, followed by washes in H_2O and then PBS. The embryos were incubated with 3% BSA in PBST (PBS with 0.1% tween 20) for at least 1 h at room temperature before overnight incubation at 4 °C with the anti-acetylated-α-tubulin Rabbit mAb, followed by washes and either Alexa 594- or Alexa 588- conjugated anti-rabbit secondary antibody in PBST (Cell Signaling Technology, Danvers, MA, USA). The next day, the embryos were washed with PBST at least three times, 15 min/each, then stored in PBS at 4 °C.

Institutional Review Board Statement: The animal study protocol was approved by the Institutional Animal Care and Use Committee (IACUC) of University of Wisconsin-River Falls (A15-16-13/8 February 2016).

Informed Consent Statement: Not applicable.

Conflicts of Interest: The authors declare no conflict of interest.

References

1. Seyfried, T.N.; Huysentruyt, L.C. On the origin of cancer metastasis. *Crit. Rev. Oncog.* **2013**, *18*, 43–73. [CrossRef] [PubMed]
2. Valent, P.; Bonnet, D.; De Maria, R.; Lapidot, T.; Copland, M.; Melo, J.V.; Chomienne, C.; Ishikawa, F.; Schuringa, J.J.; Stassi, G.; et al. Cancer stem cell definitions and terminology: The devil is in the details. *Nat. Rev. Cancer* **2012**, *12*, 767–775. [CrossRef] [PubMed]
3. Ishizawa, K.; Rasheed, Z.A.; Karisch, R.; Wang, Q.; Kowalski, J.; Susky, E.; Pereira, K.; Karamboulas, C.; Moghal, N.; Rajeshkumar, N.V.; et al. Tumor-initiating cells are rare in many human tumors. *Cell Stem Cell* **2010**, *7*, 279–282. [CrossRef] [PubMed]
4. Walcher, L.; Kistenmacher, A.-K.; Suo, H.; Kitte, R.; Dluczek, S.; Straub, A.; Blaudszun, A.-R.; Yevsa, T.; Fricke, S.; Kossatz-Boehlert, U. Cancer stem cells- origins and biomarkers: Perspectives for targeted personalized therapies. *Front. Immunol.* **2020**, *11*, 1280. [CrossRef]
5. Dalerba, P.; Clarke, M.F. Cancer stem cells and tumor metastasis: First steps into uncharted territory. *Cell Stem Cell* **2007**, *1*, 241–242. [CrossRef]
6. Vasaikar, S.V.; Deshmukh, A.P.; Hollander, P.; Addanki, S.; Kuburich, N.A.; Kudaravalli, S.; Joseph, R.; Chang, J.T.; Soundararajan, R.; Mani, S.A. EMTome: A resource for pan-cancer analysis of epithelial-mesenchymal transition genes and signatures. *Br. J. Cancer* **2021**, *124*, 259–269. [CrossRef]
7. Tania, M.; Khan, M.A.; Fu, J. Epithelial to mesenchymal transition inducing transcription factors and metastatic cancer. *Tumor Biol.* **2014**, *35*, 7335–7342. [CrossRef]
8. Chen, J.; Li, Y.; Yu, T.-S.; McKay, R.M.; Burns, D.K.; Kernie, S.G.; Parada, L.F. A restricted cell population propagates glioblastoma growth after chemotherapy. *Nature* **2012**, *488*, 522–526. [CrossRef]
9. Malladi, S.; Macalinao, D.G.; Jin, X.; He, L.; Basnet, H.; Zou, Y.; de Stanchina, E.; Massagué, J. Metastatic Latency and Immune Evasion through Autocrine Inhibition of WNT. *Cell* **2016**, *165*, 45–60. [CrossRef]
10. Kaushik, U.; Aeri, V.; Mir, S.R. Cucurbitacins—An insight into medicinal leads from nature. *Pharmacogn. Rev.* **2015**, *9*, 12–18.
11. Garg, S.; Kaul, S.C.; Wadhwa, R. Cucurbitacin B and cancer intervention: Chemistry, biology and mechanisms (Review). *Int. J. Oncol.* **2018**, *52*, 19–37. [CrossRef] [PubMed]
12. Chen, X.; Bao, J.; Guo, J.; Ding, Q.; Lu, J.; Huang, M.; Wang, Y. Biological activities and potential molecular targets of cucurbitacins: A focus on cancer. *Anti-Cancer Drugs* **2012**, *23*, 777–787. [CrossRef] [PubMed]
13. Duncan, K.L.; Duncan, M.D.; Alley, M.C.; Sausville, E.A. Cucurbitacin E-induced disruption of the actin and vimentin cytoskeleton in prostate carcinoma cells. *Biochem. Pharmacol.* **1996**, *52*, 1553–1560. [CrossRef] [PubMed]
14. Wang, X.; Tanaka, M.; Peixoto, H.S.; Wink, M. Cucurbitacins: Elucidation of their interactions with the cytoskeleton. *PeerJ* **2017**, *5*, e3357. [CrossRef] [PubMed]
15. Deng, C.; Zhang, B.; Zhang, S.; Duan, C.; Cao, Y.; Kang, W.; Yan, H.; Ding, X.; Zhou, F.; Wu, L.; et al. Low nanomolar concentrations of Cucurbitacin-I induces G2/M phase arrest and apoptosis by perturbing redox homeostasis in gastric cancer cells in vitro and in vivo. *Cell Death Dis.* **2016**, *7*, e2106. [CrossRef] [PubMed]
16. Litaudon, M.; Gaspard, C.; Sevenet, T. Morierinin: A New Cytotoxic Cucurbitacin from the Leaves of *Morierina Montana* Vieill. *Nat. Prod. Res.* **2003**, *17*, 229–233. [CrossRef]
17. Boiko, A.D.; Razorenova, O.V.; Rijn, M.V.D.; Swetter, S.M.; Johnson, D.L.; Ly, D.P.; Butler, P.D.; Yang, G.P.; Joshua, B.; Kaplan, M.J.; et al. Human melanoma-initiating cells express neural crest nerve growth factor receptor CD271. *Nature* **2010**, *466*, 133–137. [CrossRef]
18. Yin, Q.; Shi, X.; Lan, S.; Jin, H.; Wu, D. Effect of melanoma stem cells on melanoma metastasis. *Oncol. Lett.* **2021**, *22*, 566. [CrossRef]
19. Yosuoka, A.; Hirose, Y.; Yoda, H.; Aihara, Y.; Suwa, H.; Niwa, K.; Sasado, T.; Morinaga, C.; Deguchi, T.; Henrich, T.; et al. Mutations affecting the formation of posterior lateral line system in Medaka, *Oryzias latipes*. *Mech. Dev.* **2004**, *121*, 729–738. [CrossRef]

20. Schatton, T.; Murphy, G.F.; Frank, N.Y.; Yamaura, K.; Waaga-Gasser, A.M.; Gasser, M.; Zhan, Q.; Jordan, S.; Duncan, L.M.; Weishaupt, C.; et al. Identification of cells initiating human melanoma. *Nature* **2008**, *451*, 345–349. [CrossRef]

21. Quintana, E.; Shackleton, M.; Sabel, M.S.; Fullen, D.R.; Johnson, T.M.; Morrison, S.J. Efficient tumor formation by single human melanoma cells. *Nature* **2008**, *456*, 593–598. [CrossRef] [PubMed]

22. Farahani, E.; Patra, H.K.; Jangamreddy, J.R.; Rashedi, I.; Kawalec, M.; Rao Pariti, R.K.; Batakis, P.; Wiechec, E. Cell adhesion molecules and their relation to (cancer) cell stemness. *Carcinogenesis* **2014**, *35*, 747–759. [CrossRef] [PubMed]

23. Bonneau, B.; Popgeorgiev, N.; Prudent, J.; Gillet, G. Cytoskeleton dynamics in early zebrafish development. *BioArchitecture* **2011**, *1*, 216–220. [CrossRef] [PubMed]

24. Villamayor, P.R.; Arana, A.J.; Coppel, C.; Ortiz-Leal, I.; Torres, M.V.; Sanches-Quinteiro, P.; Sanches, L. A comprehensive structural, lectin and immunohistochemical characterization of the zebrafish olfactory system. *Sci. Rep.* **2021**, *11*, 8865. [CrossRef]

25. Reiten, I.; Uslu, F.E.; Fore, S.; Pelgrims, R.; Ringers, C.; Verdugo, C.D.; Hoffman, M.; Lal, P.; Kawakami, K.; Pekkan, K.; et al. Motile-cilia-mediated flow improves sensitivity and temporal resolution of olfactory computations. *Curr. Biol.* **2017**, *27*, 166–174. [CrossRef]

26. Schlaeger, N.M.; Berkan, C.; Albu, I.; Monte, A.P.; Huang, C.-C. Synthetic compounds that inhibit melanoma growth and invasiveness by reducing cancer stem cell population. *J. Cancer Biol. Res.* **2020**, *8*, 1126.

27. Westerfield, M. *The Zebrafish Book: A Guide for the Laboratory Use of Zebrafish (Danio rerio)*; University of Oregon Press: Eugene, OR, USA, 2007.

28. Haege, E.R.; Huang, H.-C.; Huang, C.-C. Identification of lactate as a cardiac protectant by inhibiting inflammation and cardiac hypertrophy using a zebrafish acute heart failure model. *Pharmaceuticals* **2021**, *14*, 261. [CrossRef]